Journal of Nuclear Materials 394 (2009) 131–135

Contents lists available at ScienceDirect

Journal of Nuclear Materials

journal homepage: www.elsevier.com/locate/jnucmat

Electrochemical formation of uranium–zirconium alloy in LiCl–KCl melts

Tsuyoshi Murakami [a,*], Tetsuya Kato [a], Masaki Kurata [a], Hajimu Yamana [b]

[a] Central Research Institute of Electric Power Industry (CRIEPI), Komae-shi, Tokyo 201-8511, Japan
[b] Research Reactor Institute, Kyoto University, Kumatori-cho, Sennan-gun, Osaka 590-0494, Japan

ARTICLE INFO

Article history:
Received 17 March 2009
Accepted 26 August 2009

ABSTRACT

Since zirconium is considered an electrochemically active species under practical conditions of the electrorefining process, it is crucial to understand the electrochemical behavior of zirconium in LiCl–KCl melts containing actinide ions. In this study, the electrochemical codeposition of uranium and zirconium on a solid cathode was performed. It was found that the δ-(U, Zr) phase, which is the only intermediate phase of the uranium–zirconium binary alloy system, was deposited on a tantalum substrate by potentiostatic electrolysis at −1.60 V (vs. Ag^+/Ag) in LiCl–KCl melts containing 0.13 in mol% UCl_3 and 0.23 in mol% $ZrCl_4$ at 773 K. To our knowledge, this is the first report on the electrochemical formation of the δ-(U, Zr) phase. The relative partial molar properties of uranium in the δ-(U, Zr) phase were evaluated by measuring the open-circuit-potentials of the electrochemically prepared δ-phase electrode.

1. Introduction

The metallic fuel cycle consisting of metallic fuel loaded in fast breeder reactor, pyrochemical reprocessing and fuel fabrication by injection casting is one of the most promising nuclear fuel cycles for the next generation because it is expected to be highly resistant against nuclear proliferation and to be economically competitive [1,2]. The major step in pyrochemical reprocessing is the electrorefining process. Fig. 1 illustrates the overall concept of the electrorefining process. Eutectic LiCl–KCl melts are used as the electrolyte at 773 K. Cut and chopped spent metallic fuels (U–Zr or U–Pu–Zr) are placed in metallic anode baskets and immersed in the eutectic LiCl–KCl melt containing actinide ions. Actinides in the fuel dissolve anodically in the melts and are recovered as a cathodic deposit.

Zirconium is a constituent of the metallic fuel and is generally present at up to 10 wt.%. The standard potential of Zr^{4+}/Zr is reported to be more positive than those of actinides such as U^{3+}/U, Pu^{3+}/Pu, Np^{3+}/Np and Am^{2+}/Am in LiCl–KCl melts [3–7]. This means that zirconium theoretically remains in the anode basket with noble metal fission products and the cladding during electrolysis as far as anodic potential is kept more negative than the dissolution potential of zirconium. On the other hand, the practical operation for the electrorefining process requires both the anodic dissolution of actinides with a high current density and a high dissolution ratio of actinides (e.g., U: >99.5%, Pu: >99.9%, minor actinides: >99.9%) at the end of electrolysis. In such a practical case, anodic potential should be kept much more positive than the dissolution potential of actinides and even zirconium. Thus, a portion of zirconium is also oxidized to form zirconium ion in the melts during electrolysis [8–12], and the formed zirconium ion is reduced on the solid cathode together with uranium. According to the phase diagram of the uranium–zirconium binary system, the α-uranium, α-zirconium, and δ-(U, Zr) phases exist at 773 K [13]. The δ-(U, Zr) phase is a nonstoichiometric alloy. Since the solubilities of uranium and zirconium are less than 0.5 at.% in α-zirconium and α-uranium, respectively, the δ-(U, Zr) phase is expected to form as the only intermediate phase during the codeposition of uranium and zirconium. Although several researches on the electrochemical behavior of uranium and zirconium in LiCl–KCl melts containing respective ion have been reported [14–18], no details have been given yet in LiCl–KCl melts containing both uranium and zirconium ions to elucidate electrochemical formation of the δ-(U, Zr) phase. Meanwhile, thermodynamic evaluations such as CALPHAD method have been performed for the uranium–zirconium and uranium–plutonium–zirconium systems to understand phase transitions in metallic fuel under irradiation [19–21]. Phase boundary data and thermodynamic properties are used in such thermodynamic evaluations. In particular, chemical activity data in the δ-(U, Zr) phase are necessary to improve the accuracy of the evaluations. However, there have been no reliable experimental values reported with respect to the δ-(U, Zr) phase yet.

In this study, therefore, several electrochemical measurements (i.e., cyclic voltammetry, potentiostatic electrolysis and open-circuit-potential measurement) were performed in LiCl–KCl melts containing uranium and zirconium ions to investigate the electrochemical formation and thermodynamic properties of the δ-(U, Zr) phase.

* Corresponding author. Tel.: +81 3 3480 2111; fax: +81 3 3480 7956.
E-mail address: m-tsuyo@criepi.denken.or.jp (T. Murakami).

0022-3115/$ - see front matter © 2009 Elsevier B.V. All rights reserved.
doi:10.1016/j.jnucmat.2009.08.016

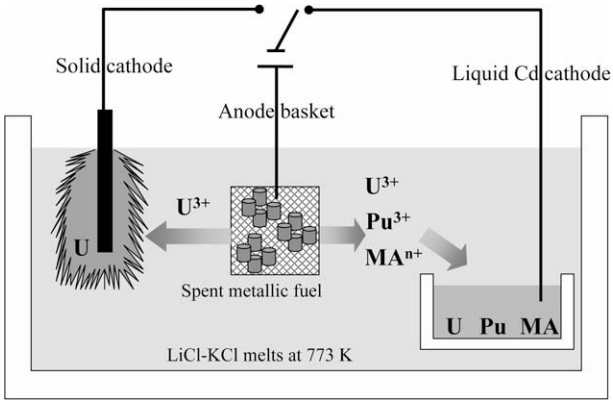

Fig. 1. Representation of principle of electrorefining process.

2. Experimental

Fig. 2 shows the experimental apparatus used in this study. All the experiments were conducted in a purified argon glove box under atmospheric pressure. The concentrations of moisture and oxygen in the glove box were controlled to be less than 1 ppm. A high-purity LiCl–KCl eutectic reagent (99.99% purity, LiCl:KCl = 58.8:41.2 in mol%, m.p. 625 K) purchased from Anderson Physics Laboratory (APL) was melted in an alumina crucible (ϕ50 mm, SSA-S, Nikkato Co., Ltd.) and used as the electrolyte at 773 K. In order to prepare LiCl–KCl–UCl_3 melts, $CdCl_2$ (99.999% purity, APL) was added to LiCl–KCl melts in which a uranium metal was immersed. UCl_3 was formed chemically in the melts according to

$$U + 3/2CdCl_2 \rightarrow UCl_3 + 3/2Cd. \quad (1)$$

In the same way, LiCl–KCl–UCl_3–$ZrCl_4$ melts were prepared by adding $CdCl_2$ to LiCl–KCl–UCl_3 melts in which a zirconium metal was immersed and reacted as,

$$Zr + 2CdCl_2 \rightarrow ZrCl_4 + 2Cd. \quad (2)$$

A previous research showed that the average valence of zirconium ion at 773 K was 3.98, which was calculated from the weight loss of the zirconium anode after the galvanostatic anodic dissolution of zirconium [14]. This suggests that the main zirconium ion species is considered to be Zr^{4+} in this study as well as in the previous research.

A tantalum wire (ϕ1 mm, 99.95% purity, Rare Metallic Co., Ltd.) was used as the working electrode for cyclic voltammetry, and a tantalum plate (5 mm × 10 mm × 1 mm, 99.95% purity, Rare Metallic Co., Ltd.) or a zirconium plate (5 mm × 10 mm × 1 mm, 99.95% purity, Rare Metallic Co., Ltd.) was used as the working electrode for potentiostatic electrolysis. Tantalum was selected as the electrode material because it is inert to uranium and zirconium. The counter electrode was a zirconium plate (5 mm × 15 mm × 1 mm) for cyclic voltammetry and potentiostatic electrolysis. The reference electrode was Ag/AgCl electrode consisting of a silver wire immersed in LiCl–KCl eutectic melts containing 1.0 wt.% AgCl (99.9% purity, APL), which was placed in a Pyrex tube with a thin bottom to maintain electrical contact with the electrolyte. A thin Pyrex glass works as an ion conducting membrane [22]. Electrochemical measurements were performed using model 273 potentiostat/galvanostat of EG&G Princeton Applied Research and EG&G M270 computer software.

The sample melts were analyzed by inductively coupled plasma-atomic emission spectrometry (ICP-AES) to measure the concentrations of UCl_3 and $ZrCl_4$ in the melts. Deposits were pulled out of the furnace immediately after electrolysis for quick cooling and rinsed with distilled water to remove residual salts. Then they were analyzed by X-ray diffraction measurement (XRD) and scanning electron microscopy–energy dispersive spectroscopy (SEM–EDS).

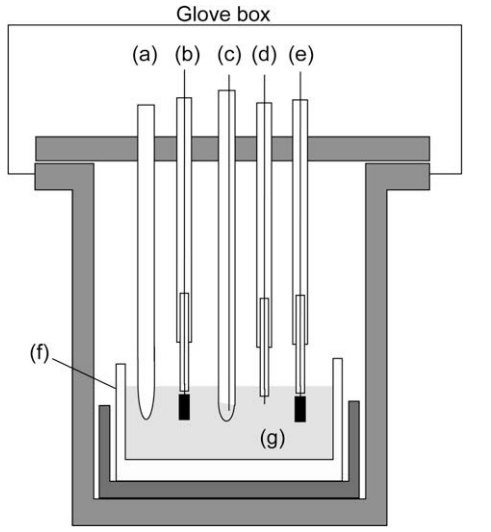

Fig. 2. Schematic drawing of experimental apparatus. (a) Thermocouple, (b) counter electrode (zirconium plate), (c) reference electrode (Ag^+/Ag), (d) working electrode (tantalum wire), (e) working electrode (tantalum or zirconium plate), (f) Al_2O_3 crucible and (g) electrolyte (eutectic LiCl–KCl melts containing UCl_3 or both UCl_3 and $ZrCl_4$).

3. Results and discussion

3.1. Cyclic voltammetry

Cyclic voltammetry using a tantalum wire was conducted in LiCl–KCl melts (Fig. 3a) and LiCl–KCl melts containing 0.13 in mol% UCl_3 (Fig. 3b). In cyclic voltammogram (a), only a couple of cathodic and anodic peaks is observed at approximately −2.44 V (vs. Ag^+/Ag), which is ascribed to lithium metal deposition and its dissolution, respectively. This shows that the amount of impurities in the melts such as water is negligible. In cyclic voltammogram (b), a sharp cathodic peak and a corresponding anodic peak are observed at approximately −1.45 V. The cathodic and anodic peaks are ascribed to the reduction of U^{3+} to uranium metal (reaction 3) and the dissolution of deposited uranium metal (reaction 4), respectively [15–18].

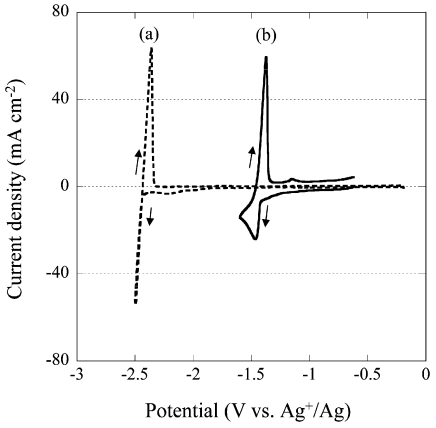

Fig. 3. Cyclic voltammograms using tantalum wire measured in (a) LiCl–KCl melts and (b) LiCl–KCl–UCl_3(0.13 in mol%) melts. The scan rate was 50 mV s^{-1}.

$$U^{3+} + 3e^- \rightarrow U, \quad (3)$$

$$U \rightarrow U^{3+} + 3e^- \quad (4)$$

Another couple of the cathodic current increasing from approximately −1.3 V and the small anodic current peak at −1.15 V is also observed. Several studies have also shown the similar cathodic and anodic current couple other than that for U^{3+}/U using several types of working electrodes (i.e., molybdenum, tungsten and carbon) in LiCl–KCl–UCl_3 melts or NaCl–KCl–UCl_3 melts [15–18]. According to these studies, it might be related to the monolayer adsorption and desorption of uranium or to the redox reaction between adsorbed U^{3+} and uranium sub-chloride.

Cyclic voltammetry using a tantalum wire was then performed in LiCl–KCl melts containing both UCl_3(0.13 in mol%) and $ZrCl_4$(0.24 in mol%). The result is given in Fig. 4. In comparison with Fig. 3b, a couple of large cathodic (peak A) and anodic (peak A′) peaks appears at approximately −1.0 V, which is due to the existence of $ZrCl_4$ in the melt. According to a previous research [14], peak A at −1.10 V is ascribed to zirconium metal deposition,

$$Zr^{4+} + 4e^- \rightarrow Zr, \quad (5)$$

and peak A′ at approximately −0.90 V corresponds to the following series of oxidation reactions

$$Zr \rightarrow Zr^{4+} + 4e^-, \quad (6)$$

$$Zr \rightarrow Zr^{2+} + 2e^-, \quad (7)$$

$$Zr^{2+} \rightarrow Zr^{4+} + 2e^-. \quad (8)$$

The reduction of Zr^{4+} to Zr^{2+} might be shown as cathodic current increasing gradually from the rest potential (−0.95 V) in a shoulder of peak A [14].

$$Zr^{4+} + 2e^- \rightarrow Zr^{2+}. \quad (9)$$

At around the uranium metal deposition potential, a broad cathodic peak (peak B) and a small anodic peak (peak B′) are observed, while the sharp anodic peak, which is observed in the cyclic voltammogram in Fig. 3b and is ascribed to uranium metal dissolution, disappears. During the cathodic scan in the potential region more negative than the zirconium metal deposition potential, the surface of the working electrode should be covered with zirconium metal deposited according to reaction 5. Therefore, the cathodic reaction at peak B is speculated to be related to the reduction of U^{3+} occurring mainly on an electrodeposited zirconium metal. The cathodic current relating to peak B in Fig. 4 increases from a potential slightly more positive than that of uranium metal deposition in the melts containing only UCl_3 shown in Fig. 3b. This implies that uranium becomes stabilized on the zirconium surface to form the δ-(U, Zr) phase electrochemically according to

$$U^{3+} + xZr + 3e^- \rightarrow \delta\text{-}(U, Zr). \quad (10)$$

The broadening of peak B is consistent with the wide nonstoichiometric composition range of the δ-(U, Zr) phase. The small anodic peak (peak B′) at approximately −1.35 V seems to correspond to peak B and to be ascribed to the oxidation of the δ-(U, Zr) phase,

$$\delta\text{-}(U, Zr) \rightarrow U^{3+} + xZr + 3e^-. \quad (11)$$

3.2. Potentiostatic electrolysis at −1.30 V and −1.60 V

In order to confirm the δ-(U, Zr) phase formation, potentiostatic electrolysis was conducted at −1.30 V and −1.60 V in LiCl–KCl–UCl_3(0.13 in mol%)–$ZrCl_4$(0.23 in mol%) melts using a tantalum plate as the working electrode. In the case of potentiostatic electrolysis at −1.30 V for 3 h, cathodic current increased gradually from −10 to −30 mA cm^{-2} during the electrolysis, implying the continuous increase in electrode surface area. After the electrolysis, black powdery deposits on the substrate were obtained. They poorly adhered to the substrate. Fig. 5a shows the XRD pattern of the deposits. All peaks of the XRD pattern, except the small peak due to the electrolyte component of KCl, are ascribed to zirconium metal. This means that only zirconium metal is deposited by potentiostatic electrolysis at −1.30 V according to reaction 5.

Fig. 6 shows the cathodic current change with respect to the duration of the potentiostatic electrolysis at −1.60 V. Cathodic current continuously increased from approximately −170 to −240 mA cm^{-2}. This indicates the increase in electrode surface area during the electrolysis. After the electrolysis, black paste-like deposits on the tantalum substrate were obtained. The adhesion of the deposits to the substrate was found to be poor. The result of the XRD analysis of the deposits (Fig. 5b) shows that two-phases exist in the deposits; the δ-(U, Zr) phase and zirconium metal. Since there are no peaks in the XRD pattern ascribed to uranium metal, it is implied that the cathodic current peak corresponding to uranium metal deposition might not overlap with peak B in cyclic voltammogram in Fig. 4.

Fig. 7 shows a SEM image of the deposits obtained after the potentiostatic electrolysis at −1.60 V. It is found that the deposits grow dendritically, which causes the continuous cathodic current increase shown in Fig. 6. Uranium concentration was analyzed at

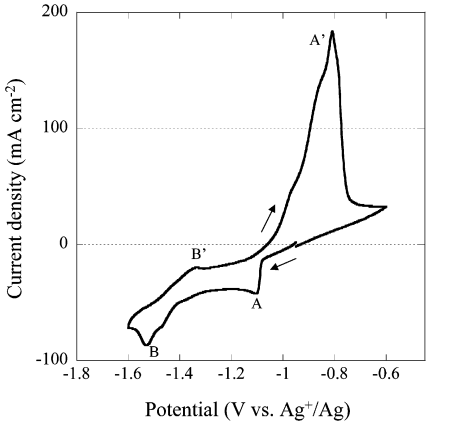

Fig. 4. Cyclic voltammogram using tantalum wire measured in LiCl–KCl–UCl_3(0.13 in mol%)–$ZrCl_4$(0.23 in mol%) melts. The scan rate was 50 mV s^{-1}.

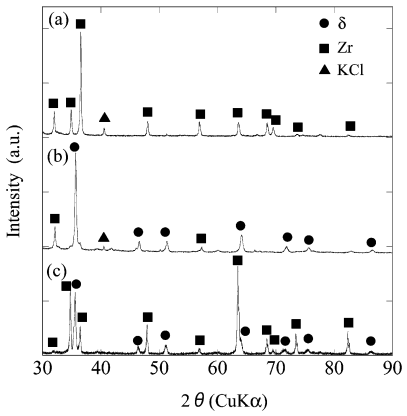

Fig. 5. XRD patterns of deposits obtained (a) after potentiostatic electrolysis at −1.30 V using the tantalum substrate in LiCl–KCl–UCl_3(0.13 in mol%)–$ZrCl_4$(0.23 in mol%) melts, (b) after potentiostatic electrolysis at −1.60 V using tantalum substrate in LiCl–KCl–UCl_3(0.13 in mol%)–$ZrCl_4$(0.23 in mol%) melts and (c) after potentiostatic electrolysis at −1.60 V using the zirconium substrate in LiCl–KCl–UCl_3(0.13 in mol%)–$ZrCl_4$(0.05 in mol%) melts.

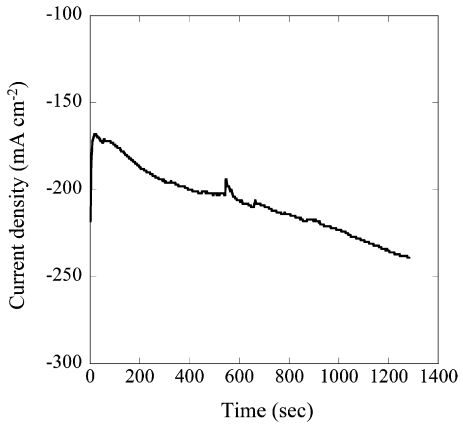

Fig. 6. Current–time curve for potentiostatic electrolysis at −1.60 V in LiCl–KCl–UCl_3(0.13 in mol%)–$ZrCl_4$(0.23 in mol%) melts.

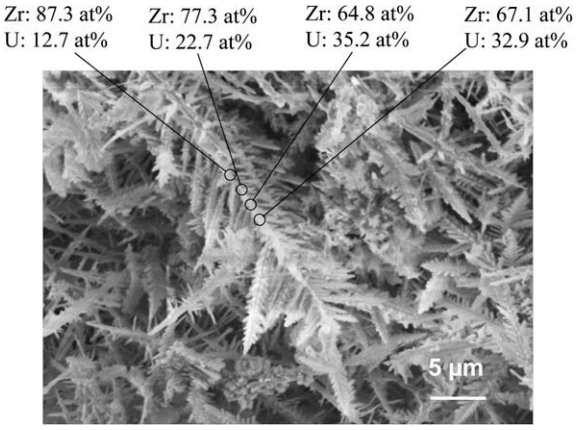

Fig. 7. SEM image and EDS analysis results of deposits obtained after potentiostatic electrolysis at −1.60 V in LiCl–KCl–UCl_3(0.13 in mol%)–$ZrCl_4$(0.23 in mol%) melts.

several points of the dendrite by EDS point analysis. As shown in Fig. 7, the uranium concentrations range from 12.7 to 35.2 at.% U. According to the phase diagram of the uranium–zirconium binary system, the nonstoichiometric composition range of the δ-(U, Zr) phase is 22–34 at.% U, although the boundary between the δ-(U, Zr) single-phase and (δ-(U, Zr) + α-zirconium) two-phase region has not been determined clearly as shown in the dotted line in the phase diagram [13]. These imply that the dendrite deposits are composed of the δ-(U, Zr) phase and α-zirconium, which agrees with the XRD results in Fig. 5b. Putting together the results of potentiostatic electrolysis at −1.30 V and −1.60 V, it is concluded that the broad peak B in the cyclic voltammogram in Fig. 4 corresponds to the δ-(U, Zr) phase formation.

3.3. Thermodynamic properties of the δ-(U, Zr) phase

As mentioned above, it is possible to form an electrode consisting of the δ-(U, Zr) phase and α-zirconium by potentiostatic electrolysis at −1.60 V in LiCl–KCl melts containing both uranium and zirconium ions. In this section, the thermodynamic properties of the δ-(U, Zr) phase coexisting with α-zirconium are evaluated by measuring the open-circuit-potential of the electrochemically prepared δ-phase electrode.

Firstly, the δ-phase electrode was prepared by potentiostatic electrolysis at −1.60 V in LiCl–KCl–UCl_3(0.13 in mol%)–$ZrCl_4$(0.05 in mol%) melts using a zirconium plate as the working electrode. Fig. 5c shows the XRD pattern indicating that the surface of the prepared δ-phase electrode consists of the δ-(U, Zr) and α-zirconium phases. Then, the open-circuit-potential of the δ-phase electrode was measured in another melt, LiCl–KCl–UCl_3(0.024 in mol%) melts, to obtain the chemical activity of uranium in the δ-(U, Zr) phase. The reference electrode was the U^{3+}/U electrode prepared by electrodepositing uranium metal on a tantalum wire in the same melt. The potential was measured with increasing and decreasing temperature in the range from 700 to 839 K with an accuracy of ±0.005 mV. It is assumed that the δ-(U, Zr) phase and α-zirconium in the electrode would reach equilibrium at each temperature.

The potentials of the δ-phase electrode measured with increasing and decreasing temperature are plotted against temperature in Fig. 8; the potentials are represented by solid and hollow circles, respectively. As shown in Fig. 8, the potentials decreased almost linearly from 5.71 mV (vs. U^{3+}/U) to 1.82 mV with an increase in temperature. The open-circuit-potential (E vs. U^{3+}/U) is expressed as

$$E = \frac{RT}{3F}\ln\frac{1}{a_U}, \tag{12}$$

where F is the Faraday constant, R is the gas constant, T is the absolute temperature, and a_U is the activity of uranium in the δ-(U, Zr) phase in equilibrium with α-zirconium. The activity of uranium and the relative partial molar properties of uranium in the δ-(U, Zr) phase; Gibbs energy ($\Delta\bar{G}_U$), entropy ($\Delta\bar{S}_U$), enthalpy ($\Delta\bar{G}_U$), are related to the open-circuit-potential of the δ-phase electrode (E) by the following equations. The reference state of these values is defined as α-uranium at each temperature.

$$a_U = \exp\left(\frac{\Delta\bar{G}_U}{RT}\right), \tag{13}$$

$$\Delta\bar{G}_U = -3FE, \tag{14}$$

$$\Delta\bar{S}_U = 3F\frac{dE}{dT}, \tag{15}$$

$$\Delta\bar{H}_U = \Delta\bar{G}_U + T\Delta\bar{S}_U. \tag{16}$$

Table 1 summarizes the activity of uranium and the relative partial molar properties of uranium in the δ-(U, Zr) phase. $\Delta\bar{S}_U$ and $\Delta\bar{H}_U$ are calculated from the slope of the regression line in Fig. 8. Fig. 9 shows the activity obtained experimentally in this study together with the simulated values obtained by Ogawa and Iwai [19] and Kurata et al. [20]. Note that differences lie between them. The simulated values in Ref. [19] are in almost the same

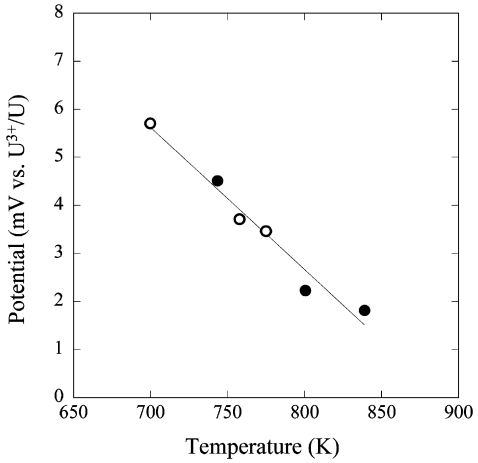

Fig. 8. Temperature dependence of open-circuit-potentials of the δ-phase electrode measured with increasing and decreasing temperature; potentials are represented by solid and hollow circles, respectively.

Table 1
Relative partial molar properties (i.e., Gibbs energy, enthalpy and entropy) of uranium and uranium activity in the δ-(U, Zr) phase with open-circuit-potentials of the δ-phase electrode. The reference state is α-uranium at each temperature.

T (K)	E (mV vs. U^{3+}/U)	$\Delta\bar{G}_U$ (kJ mol^{-1}U)	a_U	$\Delta\bar{S}_U$ (J K^{-1} mol^{-1}U)	$\Delta\bar{H}_U$ (kJ mol^{-1}U)
700	5.71	−1.65	0.753		
744	4.51	−1.31	0.810		
758	3.71	−1.07	0.843		
775	3.46	−1.00	0.856	−8.56	−7.62
801	2.23	−0.645	0.908		
839	1.82	−0.527	0.927		

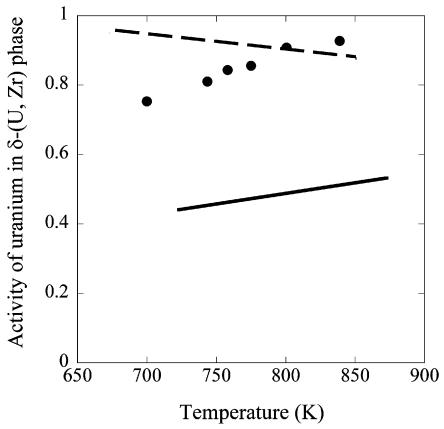

Fig. 9. Temperature dependence of activity of uranium in the δ-(U, Zr) phase. Experimental values obtained in this study (●), simulated values obtained by Ogawa and Iwai [19] (dotted line) and Kurata et al. [20] (solid line). The reference state of uranium activity is α-uranium at each temperature.

range as the present data points. However, they decrease with temperature, while the present ones increase. The simulated values in Ref. [20], in contrast, have the same temperature dependence but are smaller than the present data points. By using present values, the thermodynamic evaluation is expected to be improved. One of the authors is revising the interaction parameters of his thermodynamic modeling for the uranium–zirconium system, which will be reported in the future [23].

4. Conclusions

Electrochemical measurements by cyclic voltammetry, potentiostatic electrolysis and open-circuit-potential measurement were performed in LiCl–KCl melts containing uranium and zirconium ions. In the cyclic voltammogram measured in LiCl–KCl melts containing 0.13 in mol% UCl_3 and 0.24 in mol% $ZrCl_4$, a cathodic peak at approximately −1.10 V (vs. Ag^+/Ag), which was ascribed to zirconium metal deposition, and a broad cathodic peak at −1.41 to −1.55 V were observed. Since the current of the broad cathodic peak increased from a potential slightly more positive than that of uranium metal deposition in the melts containing only UCl_3, it was speculated that uranium was stabilized on the previously electrodeposited zirconium metal by electrochemically forming the δ-(U, Zr) phase, which is the only intermediate phase in the uranium–zirconium binary alloy system. Potentiostatic electrolysis at −1.60 V was conducted in LiCl–KCl–UCl_3(0.13 in mol%)–$ZrCl_4$(0.23 in mol%) melts. XRD analysis and SEM–EDS of the obtained deposits confirmed that the δ-(U, Zr) phase was formed with α-zirconium by the electrolysis. The open-circuit-potential of the δ-(U, Zr) phase coexisting with α-zirconium was measured in LiCl–KCl–UCl_3(0.024 in mol%) melts with reference to the U^{3+}/U electrode at 700–839 K. From the measured potentials, the relative partial molar properties of uranium in the δ-(U, Zr) phase were evaluated. By using the thermodynamic properties of the δ-(U, Zr) phase obtained in this study, it is strongly expected that the thermodynamic evaluation of metallic fuels will be revised in the future.

Acknowledgements

This work was performed at the Research Reactor Institute, Kyoto University. The authors express great thanks to Dr. T. Fujii, Dr. A. Uehara and the staffs of the Research Reactor Institute, Kyoto University for their support and helpful discussion. The authors also wish to thank Dr. T. Koyama for his helpful advice.

References

[1] Y.I. Chang, Nucl. Technol. 88 (1989) 129.
[2] T. Inoue, H. Tanaka, Proceedings of GLOBAL '97, Yokohama, Japan, October 5–10, 1997, p. 646.
[3] M.W. Chase Jr. (Ed.), NIST-JANAF Thermochemical Tables, third ed., Part 1, Am. Chem. Soc., New York, 1985.
[4] J.J. Roy, J.F. Grantham, D.L. Grimmett, S.P. Fusselman, C.L. Krueger, T.S. Storvick, T. Inoue, Y. Sakamura, N. Takahashi, J. Electrochem. Soc. 147 (1996) 2487.
[5] Y. Sakamura, O. Shirai, T. Iwai, Y. Suzuki, J. Electrochem. Soc. 147 (2) (2000) 642.
[6] Y. Sakamura, O. Shirai, T. Iwai, Y. Suzuki, J. Alloys Compd. 321 (2001) 76.
[7] J. Serp, P. Chamelot, S. Fourcaudot, R.J.M. Konings, R. Malmbeck, C. Pernel, J.C. Poignet, J. Rebizant, J.-P. Glatz, Electrochim. Acta 51 (2006) 4042.
[8] S.X. Li, T.A. Johnson, B.R. Westphal, K.M. Goff, R.W. Benedict, Proceedings of GLOBAL 2005, Tsukuba, Japan, October 9–13, 2005, paper no. 487.
[9] R.K. Ahluwalia, T.Q. Hua, H.K. Geyer, Nucl. Technol. 133 (2001) 103.
[10] M.J. Steindler, P.A. Nelson, J.E. Battles, D.W. Green, Chemical Tecnology Division Annual Technical Report 1991 ANL-92/15.
[11] K. Kinoshita, T. Koyama, T. Inoue, M. Ougier, J.-P. Glatz, J. Phys. Chem. Solids 66 (2005) 619.
[12] M. Iizuka, K. Uozumi, T. Ogata, T. Omori, T. Tsukada, J. Nucl. Sci. Technol. 46 (2009) 699.
[13] T.B. Massalski (Ed.), Binary Phase Diagram, American Society for Metals, Metals Park, Ohio 44073, 1986.
[14] Y. Sakamura, J. Electrochem. Soc. 151 (3) (2004) C187.
[15] O. Shirai, T. Iwai, Y. Suzuki, Y. Sakamura, H. Tanaka, J. Alloys Compd. 271–273 (1998) 685.
[16] K. Serrano, P. Taxil, J. Appl. Electrochem. 29 (1999) 497.
[17] B.P. Reddy, S. Vandarkuzhali, T. Subramanian, P. Venkatesh, Electrochim. Acta 49 (2004) 2471.
[18] P. Masset, D. Bottomley, R. Konings, R. Malmbeck, A. Rodrigues, J. Serp, J.-P. Glatz, J. Electrochem. Soc. 152 (6) (2005) A1109.
[19] T. Ogawa, T. Iwai, J. Less-Common Met. 170 (1990) 101.
[20] M. Kurata, T. Ogata, K. Nakamura, T. Ogawa, J. Alloys Compd. 271 (1998) 636.
[21] M. Kurata, Calphad 23 (1999) 305.
[22] L. Yang, R.G. Hudson, J. Electrochem. Soc. 106 (11) (1959) 986.
[23] M. Kurata, Proceeding of Actinides 2009, July 12–17 2009, San Francisco, USA, in press.